ARTICLE

BIOTECHNOLOGY and BIOENGINEERING

Effective Diffusivities and Mass Fluxes in Fungal Biopellets

A. Hille,[1,2] T.R. Neu,[3] D.C. Hempel,[2] H. Horn[1]

[1]Institute of Water Quality Control, Technische Universität München, Am Coulombwall, D-85748 Garching, Germany; telephone: 49-89-289-13701; fax: 49-89-13718; e-mail: a.hille@bv.tum.de

[2]Institute of Biochemical Engineering, Technische Universität Braunschweig, Braunschweig, Germany

[3]Department of River Ecology, Helmholtz Centre for Environmental Research — UFZ, Magdeburg, Germany

Received 4 July 2008; revision received 28 March 2009; accepted 31 March 2009

Published online 9 April 2009 in Wiley InterScience (www.interscience.wiley.com). DOI 10.1002/bit.22351

ABSTRACT: Mass transport within biological aggregates is a key process that can determine overall turnover rates in submerged cultivations. A parameter commonly used for its description is the effective diffusion coefficient D_{eff}, which is highly dependent on biomass density and structure. Different approaches have been used to estimate or measure D_{eff}, yet the data still shows broad scattering. This study provides experimental data on effective diffusivities of oxygen within fungal pellets. A correlation is found with the hyphal gradient (dh/dr), which is a morphological parameter describing the structure of the pellet periphery. Furthermore, the dependency of D_{eff} on fluid dynamic conditions at the pellet is investigated. The comparison of the results with data from literature clearly demonstrates the influence of the experimental methodology applied for determination of D_{eff}. Moreover, it is shown that while diffusion limitation of whole pellets is mainly a function of size, the influence of advection in the outer zone of pellets that is supplied with oxygen is actually rather high. Thus, it is concluded that the effective diffusion coefficient might not be sufficient for the description of mass transport within the pellet periphery for a broad range of realistic fluid dynamic conditions during cultivation. Nevertheless, although actual mass transport rates inside pellets are unknown, mass fluxes can be calculated on the basis of spatially resolved data of oxygen and biomass distribution within the pellet.

Biotechnol. Bioeng. 2009;103: 1202–1213.

KEYWORDS: effective diffusion coefficient; *Aspergillus niger*; mass transport; microelectrode; CLSM

Introduction

The topic of mass transfer resistance in biological aggregates such as fungal pellets has been discussed for decades. Nevertheless, a great number of questions concerning mass transport properties are still not answered satisfactorily. In this work, we focus on the fate of oxygen as a limiting substrate in submerged pellet cultivations of fungi. In these cultivations the biomass productivity can be limited by both mass transfer of substrate from the bulk phase to the phase boundary as well as by mass transfer within the filamentous structure. The penetration depth of substrate and thus, fraction of pellet biomass which contributes to turnover and production, is directly linked to mass transfer within these two regions. The effective diffusion coefficient D_{eff} is a parameter widely used in equations for the description and calculation of mass transport and finally also of turnover. This approach is based on the assumption that diffusion is the dominating mass transport mechanism within pellets. Principally, the D_{eff} within a pellet depends on the space available for transport. Therefore, it is often expressed as a function of the pellet porosity ε or biomass density. By considering porosity to be the only influential parameter, several authors have been able to mathematically describe mass transport in fungal pellets (Cui et al., 1998a; Elberling and Damgaard, 2001; Escamilla Silva et al., 2001; King, 1998; Miura et al., 1975). In their works, the effective diffusion coefficient is assumed to be directly proportional to the porosity:

$$D_{eff} = \varepsilon D_{mol} \quad (1)$$

Although this equation only considers the aggregate's radial paths, the results do not deviate significantly from those obtained with empirical equations accounting for the

Correspondence to: A. Hille

Contract grant sponsor: German Research Foundation

Contract grant number: SFB 578

pore connectedness (tortuosity) (Riley et al., 1995) or influence of advective transport within the particle (Sharon et al., 1999).

To account for the set of conditions under which the effective diffusion coefficient is determined and to provide a parameter that can be compared between different sets of conditions (e.g., type of diffusing molecule, type of medium and temperature) the diffusion factor f_D can be used. It is defined as the ratio of the effective diffusion coefficient to the molecular one in the liquid phase D_{mol}. Values of f_D are reported to range between 0.04 and 0.93 for oxygen in pellets of *Aspergillus niger* (Fan et al., 1990; Huang and Bungay, 1973; Yano et al., 1961). Various methods have been used for the determination of f_D, including interpretation of oxygen concentration profiles and application of diffusion-reaction-models based on Fick's first and second laws of diffusion. The reported data for diffusion factors in fungal pellets tends to be scattered due to the impact of morphology and fluid dynamic conditions on internal mass transport processes (Cronenberg et al., 1994). When applying the microelectrode technique to biofilms, Fu et al. (1994) and Bishop et al. (1995) also observed wide ranges of effective diffusivities and both discussed the influence of structure on mass transport and turnover.

As the biomass in fungal pellets is usually not distributed homogeneously over the pellet radius (Hille et al., 2005), the effective diffusion coefficient is likewise dependent on the radial coordinate. Cronenberg et al. (1994) measured effective diffusion coefficients for inactivated pellets of *Penicillium chrysogenum* in intensely mixed media. For young, dense pellets with rather homogeneously structured morphologies, they found the diffusion factor within to vary between 0.8 and 1. With increasing age and the development of more loosely structured pellets, a dependency of the diffusivity on the radial coordinate was shown. For these pellets it was revealed that advection contributed to mass transport. As early as the 1980s, significant evidence of the influence of advection and turbulent diffusion in the outer zones of *P. chrysogenum* pellets was reported (Wittler et al., 1984). In the mathematical model of the production of β-lactam by *P. chrysogenum* presented by Bellgardt (1998), a density-dependent effective diffusion coefficient was introduced. In the outer porous pellet zone, D_{eff} was set to a distinct value of $5 \times D_{mol}$ to account for facilitated transport by microeddies. However, the majority of models of mass transport and turnover in fungal pellets depict mass transport as being purely diffusive on the basis that advection and turbulence are negligible in submerged cultivations (Cui et al., 1998a; Escamilla Silva et al., 2001; King, 1998; Lejeune and Baron, 1997; Yano et al., 1961).

This article provides experimental data on effective diffusivities of oxygen within fungal pellets and their dependency on fluid dynamic conditions. Advective mass transport appears to play a major role in mass transport within these pellets (Hille et al., 2005), however actual transport rates remain mostly unknown. Therefore, a method is introduced for the calculation of mass fluxes on the basis of spatially resolved data of oxygen and biomass distribution within the pellet. This work is based on the investigation presented in Hille et al. (2005), where the morphology of *A. niger* pellets was quantified using confocal laser scanning microscopy (CLSM) and digital image analysis.

Materials and Methods

Strain and Cultivation

Pellets of *A. niger* AB.1.13 (Mattern et al., 1992) were cultivated in stirred tank reactors at laboratory scale as already described (Hille et al., 2005; Kelly et al., 2004). Depending on cultivation conditions, mainly energy input (agitation and aeration) and pH, different pellet morphologies were generated (Kelly et al., 2004). Glucose was supplied as a carbon source and the medium composition was as follows (amounts quoted in $g\,L^{-1}$): glucose 25, $CaCl_2$ 0.10, $MgSO_4$ 0.2, $(NH4)_2SO_4$ 1.65, KH_2PO_4 2.5, Uridine 0.244, and trace element solution $100\,\mu L\,L^{-1}$ (Kelly et al., 2004).

Pellet Morphology

Pellet Size and Density

Pellet size was determined by digital image analysis. Photos of suspended pellets were taken with a CCD-camera. The cross-sectional area of the pellets was measured with image analysis software (Zeiss KS300, version 3.0). Pellet diameter and volume were calculated assuming ideal spherical shape.

The specific biomass density of the pellets investigated (ρ_P) was determined gravimetrically as depicted in Hille et al. (2005) and defined as dry mass (m_d) per wet volume (V_P)

$$\rho_P = \frac{m_d}{V_P} \tag{2}$$

with V_P obtained from image analysis.

Radial Biomass Distribution and the Hyphal Gradient (dh/dr)—Confocal Laser Scanning Microscopy (CLSM) and Image Analysis

A negative staining with fluorescence labeled dextrane (D-3305 fluoresceine, molecular weight 3,000 Da, Molecular Probes, Eugene, OR; concentration $1\,mg\,mL^{-1}$ (dilution with deionized water)) was applied to cryomicrotome slices of 40–60 μm thickness obtained from the equatorial plane of the pellets. Images were recorded with an upright TCS SP confocal laser scanning microscope (Leica, Heidelberg, Germany), controlled by CONFOCAL software, v2.00 (Leica). Both 10×0.3 and 40×0.8 numerical aperture (NA) water immersible lenses were employed. The excitation line of the argon laser was 488 nm and fluorescence emission was detected in the range of 500–550 nm.

Samples were scanned in the x–y direction to a depth of 3–18 μm with a step size of 0.5 μm. ImageJ analyzing freeware with a self-written macro was used for image analysis (Staudt, 2005). After conversion of the image stack to binary images (assigning pixels to pore volume or hyphae), quantification was performed in the z-direction. The radial biomass distribution in a pellet was determined by pixel counts in steps of 0.5 μm within a chosen cropped region (a bandwidth of 63.5 μm, running through the core of the pellet). Biomass is expressed as volumetric hyphal fraction and is plotted versus the pellet diameter. For characterization of pellet morphology, a morphological parameter—the hyphal gradient (dh/dr)—was derived from this radial distribution of hyphal volume. This (dh/dr) is defined as the increase of hyphal volume fraction in the outer pellet zone, starting from the outer edge of the pellet and extending inwards a minimum 50 μm in depth. This minimum zone was chosen as it proved to yield a well defined gradient (with minimum scattering), even for pellets with very densely structured pellet peripheries. The depth selected for determination of the gradient is limited to the outer zone where there is a linear increase in hyphal density. For most dense pellets, after reaching a certain depth within the pellet, the hyphal density declines again. This part is not considered with (dh/dr). For rather loosely structured pellets, the gradient often can be determined along the whole radial coordinate. (dh/dr) is obtained as a linear regression of the outer part of the radial profile of hyphal distribution towards the pellet core, and is given as [% μm^{-1}]. The (dh/dr) determined was averaged from two to four analysis regions per pellet (for a detailed description see Hille et al., 2005). In a previous article it was confirmed that oxygen concentration profiles in the pellets measured with the microelectrode technique show a better correlation with this morphological parameter than with conventional, average parameters such as the mean pellet density (Hille et al., 2005). For a rough estimation of this gradient, the determination of sinking velocities of pellets and their mean biomass density proved to be sufficient (Hille, 2008).

Pellet surface structures were visualized using a protein dye (SYPRO Orange, Molecular Probes; concentration 1 μL mL^{-1}) that stains hyphal cell walls. CLSM images were recorded with a 20×0.5 NA water immersible lens at an excitation of 488 nm. Emission was detected in the range of 550–655 nm. Starting in the bulk phase above the pellet, samples were scanned in the z-direction in steps of 1 or 2 μm to a depth of ~80–170 μm. Image stacks with edge lengths of 500 μm were visualized with IMARIS, v4.0.2 software (Bitplane AG, Zuerich, Switzerland) and presented as 3-D isosurface reconstructions.

Microelectrode Measurements and Evaluation of Oxygen Profiles

Measurement equipment and setup was purchased from Unisense A/S (Aarhus C, Denmark), and includes a picoammeter (PA 2000, Unisense A/S), a motor driven micromanipulator (MM33-M, Unisense A/S) connected to a stepper (encoder mike controller 18011, Oriel, Stratford, CT), and control software (Profix, Version 2.2, Pyro Science, Aachen, Germany). Oxygen microelectrodes are of the Clark type (Revsbech et al., 2000) and also purchased from Unisense A/S. Spatially resolved oxygen profiles were measured in a special flow cell consisting of a glass tube of 1.2 m length and 2.4 cm diameter where different, well-defined hydrodynamic conditions could be adjusted. A pellet was fixed to a holder and placed in the middle of the cross-sectional area of the tube.

The microelectrode was mounted on a micromanipulator and inserted into the flow cell through a port located directly above the pellet. The microelectrode was then driven into the pellet in 10 μm increments. Oxygen profiles were measured along the equatorial plane of the pellet, perpendicular to the flow direction. During profile measurements in the flow cell, the position of the microelectrode tip could be observed with a CCD camera (PAL norm) connected to a TV monitor (Hille et al., 2005). With this, the outer edge of the pellet surface could be visually recorded with an accuracy of ±20 μm. This is of great advantage for analysis and interpretation of the oxygen concentration profiles.

A 20% dilution of the cultivation medium was used for microelectrode measurements, with a final glucose concentration of 5 g L^{-1}. Thus, oxygen was the limiting substrate within the pellet. Temperature and pH values of the investigated cultivation were adjusted. The medium was saturated with atmospheric oxygen (oxygen concentration of ~7.5 mg L^{-1}). Measurements were started half an hour after placing the pellet in the flow cell to assure a steady state had been reached (balance of oxygen transport and consumption).

When interpreting oxygen profiles determined in biological aggregates of any kind it must be considered that their slopes are the result of a combination of mass transport and mass turnover. An individual consideration of each process on the sole basis of oxygen distribution is not possible.

For the description of mass transport in biopellets, the effective diffusion coefficient D_{eff} is a commonly used parameter (refer also to Eq. 1):

$$D_{eff} = f_D D_{mol} \tag{3}$$

with the diffusion factor f_D and the molecular diffusion coefficient D_{mol}. f_D depends on pellet morphology and decreases with increasing sterical hindrance. Since the pellet porosity is unevenly distributed along the pellet radius, f_D is also a function of the radius.

Two different approaches are discussed and compared in this article. For the calculation of diffusion factors according to the classical approach based on the film theory (Lewis and Whitman, 1924) (Fick's first law, see Eq. 4), mass fluxes j_l were determined from oxygen profiles measured at laminar

flow conditions at the pellet.

$$j_l = -D_{mol}\left(\frac{dc_{O_2}}{dr}\right)_P \quad (4)$$

The slope $(dc_{O_2}/dr)_P$ was determined within the diffusion boundary layer located directly above the pellet surface. Thus, the molecular diffusion coefficient of oxygen in pure water D_{mol} can be applied and is assumed to be $2.799\ 10^{-9}\,m^2\,s^{-1}$ at 30°C (extrapolated from Andrussow, 1969). Following the law of conservation of mass, the mass flux obtained from this calculation is equal to the one entering the pellet.

$$j_l = f_D\left(-D_{mol}\left(\frac{dc_{O_2}}{dr}\right)_{max}\right) \quad (5)$$

Here, the transport is described by the combination of the effective diffusion coefficient and the maximum oxygen concentration gradient inside the pellet. By equating both fluxes, f_D (and therefrom D_{eff}) can be calculated as the only unknown variable.

$$-D_{mol}\left(\frac{dc_{O_2}}{dr}\right)_P = f_D\left(-D_{mol}\left(\frac{dc_{O_2}}{dr}\right)_{max}\right) \quad (6)$$

For all pellet morphologies investigated, the diffusion coefficients determined in preliminary work ranged between 70 and almost 100% ($0.7 < f_D < 1$) of the molecular diffusion coefficient in water. However, no significant dependence on the pellet morphology could be stated.

Therefore, for the estimation of effective diffusion coefficients two additional methods were applied. One is based on the investigation of viable pellets and the application of Fick's first law. The other is based on measurements in inactivated pellets and temporally variable diffusion (Fick's second law of diffusion).

Oxygen Uptake Kinetics

For the determination of oxygen uptake kinetics, a microkinetic-cell with a working volume of 2.3 mL was used. The cylindrical cell consists of four plates made of acrylic glass (polymethylmethacrylate). The interior (diameter 10 mm) is separated into three compartments by synthetic gauze (mesh size 355 μm). In the bottom compartment a cruciform magnetic stirrer (diameter 9 mm) mixes the reaction medium. A heat exchanger is also incorporated into this segment which tempers the medium to 30°C. The pellets were put in the middle compartment above the stirrer and oxygen measurements were performed in the top segment with a microelectrode. The electrode was inserted into the cell through a hole of 500 μm diameter in the metallic cover plate (VA steel, thickness 50 μm) via a manually operated micromanipulator (see Fig. 1). The gauze prevents mechanical damage of the pellets by the stirrer as well as damage of the microelectrode by suspended pellets.

Depending on the mean pellet size, between 20 and 100 pellets of similar diameter ($d_P \pm 150$ μm) were transferred into the cell. It was then filled with a tempered, oxygen-enriched medium (same composition as in the flow cell measurements) and sealed without air entrapment. The microelectrode was inserted into the cell and the measurement of oxygen decrease was started. The rotational speed of the stirrer was set at $19\ s^{-1}$. The resulting Reynolds numbers, which are mainly influenced by the gauze, are assumed to be in the lower transition range from laminar to turbulent flow for all particles and are therefore comparable between measurements.

Using the logger function of the Profix-software, the oxygen decrease was recorded at intervals of 10 s. Finally, pellets were withdrawn from the cell to determine their size via image analysis and their mean density. The temporally resolved oxygen decrease was fitted with a second-order polynomial to determine its slope (dc_{O_2}/dt) at saturation concentration ($7.55\ mg\,L^{-1}$). This oxygen uptake rate was

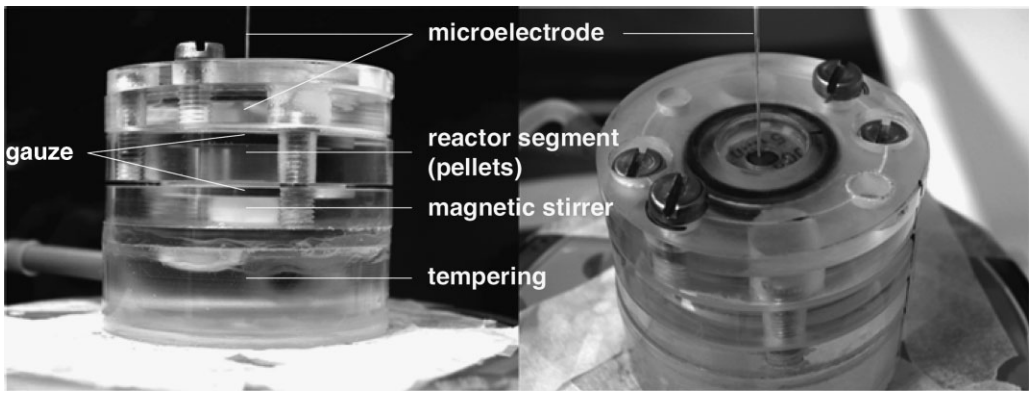

Figure 1. Microkinetic-cell, lateral and top view.

corrected by inclusion of the results from the control experiments performed without pellets. Mass flux j_{MK} was calculated as follows

$$j_{MK} = \frac{dc_{O_2}}{dt} \frac{V_{MK}}{A_P} \quad (7)$$

with the volume of the cell V_{MK} and the surface of the pellets applied A_P. V_{MK}, the volume of the liquid phase, was obtained from the difference of the cell volume and the total volume of the pellets. V_{MK} and A_P were calculated from the pellet diameters obtained through image analysis.

Determination of Effective Diffusion Coefficients in Inactivated Pellets—Stimulus–Response Experiments

For inactivation, pellets of a reactor sample were autoclaved for 20 min at 121°C. This does not influence the pellet structure as proved by CLSM-analyses before and after inactivation. Neither a reduction of hyphal volume nor an increase of the permeability of hyphal cell membranes was observed.

For determination of the effective diffusion coefficient, a pellet was fixed in the flow cell. A microelectrode was inserted radially into the pellet to a defined depth of 100 or 200 μm, respectively. A second microelectrode was driven down to the outer edge of the pellet at a small angle and positioned in front of the first electrode with respect to the flow direction (Fig. 2). The pellet surface was determined visually.

After the medium had been saturated with nitrogen, the mixing vessel was aerated with pure oxygen causing the concentration in the tube to increase sharply. This change of concentration was recorded by both electrodes in intervals of 2 s. The time shift between the increases of concentration reflects the velocity of mass transport from the pellet surface to the defined depth of the second electrode. For the calculation of the effective diffusion coefficient from the oxygen concentration profiles obtained, the simulation software AQUASIM (Reichert, 1994) was used. The model integrated into the software was already applied to simulate mass turnover and product formation in pellets of *A. niger* (Rinas et al., 2005). Thus, in this article, only the general procedure is introduced. The concentration profile measured at the pellet surface was implemented in the program as a real list. By the application of Fick's second law

$$\frac{dc_{O_2}}{dt} = D_{eff} \frac{d^2 c_{O_2}}{dr^2} \quad (8)$$

oxygen transport through the regarded pellet layer was solved numerically and a theoretical "response" concentration profile for the second electrode was calculated. Then, by means of the variable D_{eff}, the simulated curve was fitted to the actual concentration profile measured in the defined depth (see Fig. 5).

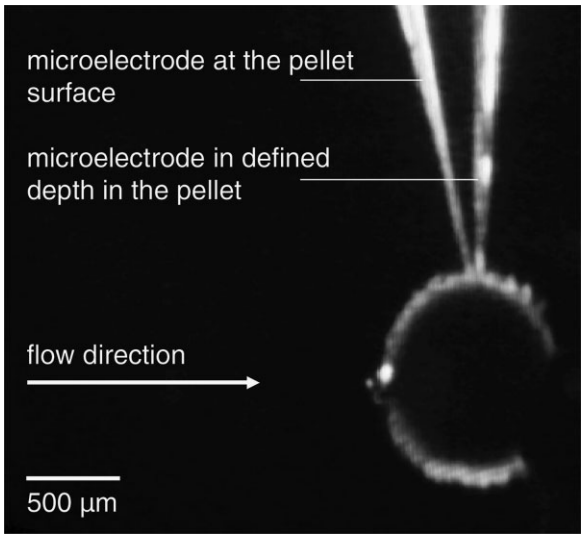

Figure 2. Measurement of D_{eff} in an inactivated pellet (photography).

Results and Discussion

Viable Pellets—Kinetics of Oxygen Uptake

This method is based on the combination of oxygen consumption kinetics and the quasi-stationary oxygen concentration profiles measured inside the pellets. It resembles closely the procedure for determining effective diffusion coefficients in biofilms introduced by Wäsche et al. (2002) and Horn and Morgenroth (2006). A major deviation of this method from the other approaches mentioned is that the kinetics and profiles cannot be measured in the same experimental setup and, thus, not at identical environmental conditions. Oxygen-consumption kinetics of 20–100 pellets of comparable size from a reactor sample are determined in the microkinetic-cell (Fig. 1). Mass fluxes are calculated at air-saturation of the broth (7.55 mg L^{-1}). Subsequently, a quasi-stationary oxygen concentration profile is recorded in a pellet of the same sample in the flow cell at a Reynolds number in the tube of $Re_{FC} = 4{,}950$ ($Re_P = 50$–500 for $d_P = 200$–$2{,}000$ μm). By equating the mass fluxes determined by micro-kinetics and oxygen profile measurements (Eqs. 5 and 7) the diffusion factor is calculated on the basis of Fick's first law of diffusion.

Figure 3 depicts the diffusion factors obtained, which are correlated with the mean pellet density to allow for the comparison with data from literature. Accordingly, this depiction is based on the assumption of a homogeneous pellet structure described by the average parameter ρ. As expected, for all pellets investigated it becomes apparent that diffusion factors decrease with increasing pellet density and thus, decreasing pore volume. The values determined in fungal pellets are generally higher than those for biofilms

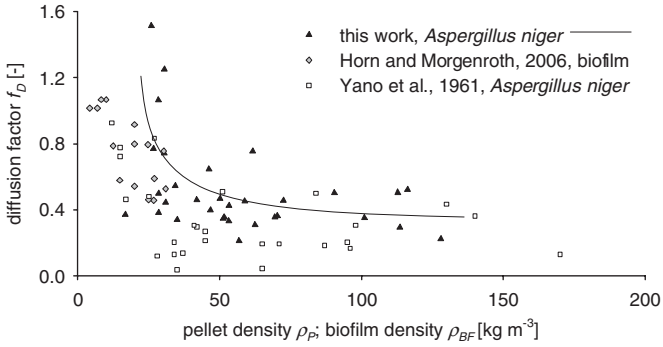

Figure 3. Diffusion factors f_D in biofilms and fungal pellets dependent on aggregate density.

(Horn and Morgenroth, 2006). This finding is not surprising since mass transfer in biofilms is not only restricted by the spatial distribution of microorganisms themselves, but also by the gel-like matrix of extracellular polymeric substances (EPS) in which the organisms are embedded (Fu et al., 1994).

At times, for pellets with biomass densities of ~25–30 kg m^{-3} diffusion factors greater than one were determined in this work. These values are ascribed to the loosely structured pellet peripheries characteristic of less dense pellets. The looser structures can experience additional mass transport mechanisms such as eddy diffusion or advection. Additionally, there were instances where much lower factors were also calculated for comparable pellet densities. For these cases it was observed that the hyphae extending into the bulk phase were significantly bent by the fluid flow to the point where they actually laid flush against the pellet surface. This leads to an enhanced local biomass density and with it, an increase of mass transfer resistance. It should be considered that the mean pellet density usually does not reflect the morphology of the periphery of the pellet where the oxygen profiles are determined (Hille et al., 2005). Nevertheless, the results obtained in this work deviate significantly from the data of Yano et al. (1961) who found much lower diffusion factors for *A. niger* pellets (Fig. 3). This indicates that the values determined with the method presented here possibly do not represent pure diffusion coefficients. It seems that hydrodynamics of the bulk phase had a significant impact on mass fluxes and maximum oxygen concentration gradients $(\mathrm{d}c_{O_2}/\mathrm{d}r)_{max}$. In contrast, the data of Yano et al. are calculated based on the determination of maximum oxygen uptake rates and solution of the mass balance. The large scattering of their values is attributed to simplifications such as homogeneous biomass distribution. Assuming that the effective diffusion coefficient can actually be described satisfactorily by the simple correlation with porosity (Eqs. 9 and 10)

$$D_{\mathrm{eff}} = \varepsilon_{\mathrm{P}} D_{\mathrm{mol}} \tag{9}$$

and

$$\frac{D_{\mathrm{eff}}}{D_{\mathrm{mol}}} = \varepsilon_{\mathrm{P}} = f_{\mathrm{D}} \tag{10}$$

porosities of the pellets investigated by Yano et al. would range between 0.04 and 0.93 (average 0.34 ± 0.24). Thus, the fraction of the hyphal volume in the pellet would range between 0.96 and 0.07. However, with regard to the maximum possible hyphal fraction, values well above 70% seem to be rather unlikely. According to the densest cylinder packing the maximum hyphal fraction would reach 90.7%, in the case of a centrical densest packing only 74%. Values in literature are usually reported to be below 50% (Cui et al., 1997; Wittler et al., 1984). Based on Equation (11), only for the maximum pellet density of 170 kg m^{-3} denoted by Yano et al. (compare Fig. 3) a hyphal fraction of 0.77 and thus a minimum diffusion factor of 0.23 would be expected, assuming a hyphal dry density ρ_{H} of 220 kg m^{-3} (this value is taken from Cui et al., 1997, assumed for *Aspergillus awamori* pellets).

$$\varepsilon_{\rho} = 1 - \frac{\rho_{\mathrm{P}}}{\rho_{\mathrm{H}}} \tag{11}$$

Considering these assumptions, the results of f_{D} obtained in this work seem to be more plausible than the ones reported by Yano et al. However, neither set of data shows a linear correlation between diffusion factor and pellet density as it should be expected according to Equations (9) and (11). In this regard, it is important to keep in mind that this again only holds true for the assumption of a homogeneous biomass distribution, which is not realistic as was shown before (El-Enshasy et al., 1999; Hamanaka et al., 2001; Higashiyama et al., 1999; Hille et al., 2005; Wittler et al., 1986).

Since the hyphal gradient ($\mathrm{d}h/\mathrm{d}r$) in the pellet periphery generally proved to be more meaningful for the assessment of mass transport and turnover than average morphological parameters (compare Hille et al., 2005), f_{D} is correlated with ($\mathrm{d}h/\mathrm{d}r$) in Figure 4. In this figure, the scattering of the trend line is slightly lower. However it is still apparent that with the chosen method, the influence of morphology on the diffusion factor cannot be detected above a hyphal gradient of ~0.4% μm^{-1} (pellet density of ~40 kg m^{-3}). For these cases, f_{D} shows no significant dependency on the hyphal gradient. As discussed before (Hille et al., 2005), the maximum oxygen concentration gradient used for the calculation of D_{eff} often is not localized at the pellet surface, but rather is deeper within the pellet. Thus, the region where $(\mathrm{d}c_{O_2}/\mathrm{d}r)_{max}$ is determined is not necessarily congruent with the one described by the morphological parameter ($\mathrm{d}h/\mathrm{d}r$). Furthermore, the influence of the flow field on $(\mathrm{d}c_{O_2}/\mathrm{d}r)_{max}$ is also different depending on pellet morphology and this consequently restricts the comparability.

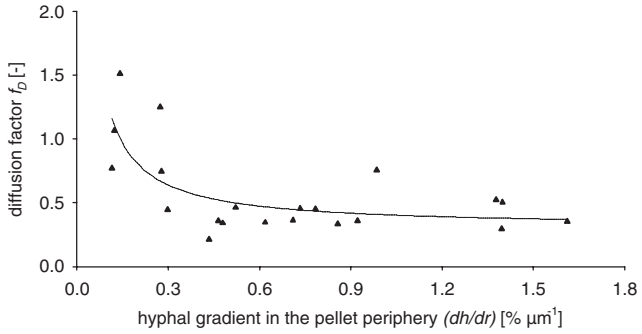

Figure 4. Diffusion factors f_D dependent on (d*h*/d*r*), determined from oxygen uptake kinetics and oxygen concentration gradients at $w_P = 0.199\,m\,s^{-1}$ ($106 < Re_P < 522$).

Inactivated Pellets—Stimulus–Response Experiments

Although the microelectrode technique is advantageous in that it provides spatially resolved oxygen concentrations within the pellets, the degree to which the oxygen concentration profile is affected by mass transport and consumption cannot be distinguished. Thus, errors arise when utilizing this technique for determining diffusion factors in active pellets since the $(dc_{O_2}/dr)_{max}$ (Eq. 5) derived from the profiles is higher than it would be as a result of mass transport only. In order to avoid the resulting underestimation of f_D, a method was applied that is based on an inactivation of pellet metabolism. In stimulus–response experiments (compare Materials and Methods Section), diffusion coefficients were determined in the periphery of pellets having densities of $18.8 < \rho_P < 96.3\,kg\,m^{-3}$. Diffusion factors were experimentally determined within two different periphery thicknesses (pellet surface to 100 µm depth and pellet surface to 200 µm depth, see Materials and Methods Section). Figure 5 shows an example of the simulation of experimental results. Here, a diffusion factor of $f_D = 0.9$ was determined for the outer layer of 200 µm thickness.

The differences between the diffusion factors determined for the two different periphery thicknesses range up to 40% (Fig. 6). As expected, it cannot be assumed that D_{eff} remains constant throughout the pellet. The inhomogeneous distribution of biomass will continue to be a restricting factor when determining effective diffusion coefficients, regardless of the experimental method applied. Here, despite the exceedingly low flow velocities resulting in laminar flow at the particle ($Re_P < 1$), advective transport still appears to occur within the outer pellet layer (100 µm) of very loosely structured pellets ($(dh/dr) < 0.5\%\,\mu m^{-1}$). As a result, diffusion factors larger than one are determined.

The dependency of the diffusion factor on the hyphal gradient at three different hydrodynamic conditions at the particle is shown in Figure 7. At flow velocities $> 0.00037\,m\,s^{-1}$, mass transport in a depth of 200 µm is greater than what would be expected by molecular diffusion ($f_D > 1$). Even in rather dense pellets ($(dh/dr) = 0.7\%\,\mu m^{-1}$), f_D is dependent on the flow velocity.

To be able to neglect hydrodynamic influence and describe the correlation between pure, effective diffusion coefficients and pellet structure, diffusion factors were determined for the outer 200 µm pellet radius at very low Reynolds numbers at the particle of $1.5 < Re_P < 2.5$. f_D ranges between 0.65 and 0.85. In Figure 8, the values found for f_D were correlated with the porosity which was determined by two different methods. One porosity was

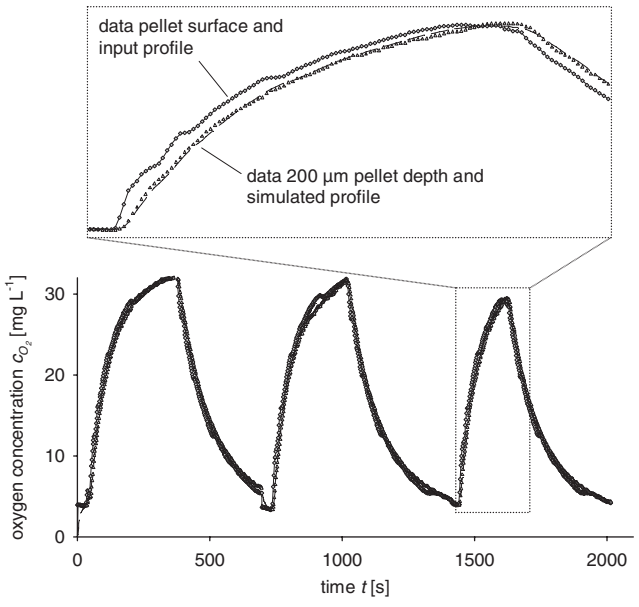

Figure 5. Example of experimental data and simulated profiles of oxygen concentration at the pellet surface and at a depth of 200 µm. Measured at $w_P = 0.199\,m\,s^{-1}$ ($Re_P = 243$).

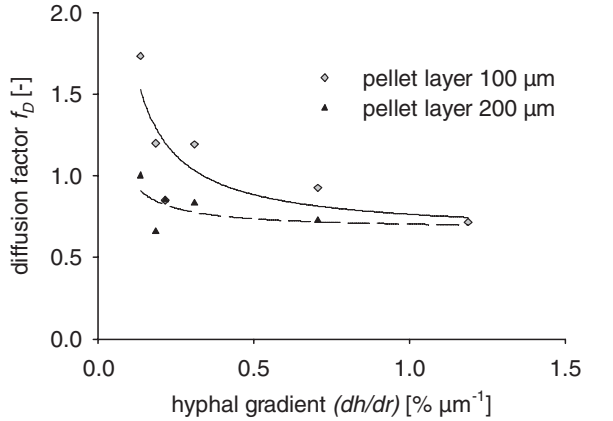

Figure 6. Diffusion factors f_D for the periphery thicknesses of 100 and 200 µm in pellets of different morphology. Measured at $w_P = 0.00037\,m\,s^{-1}$ ($Re_P < 1$).

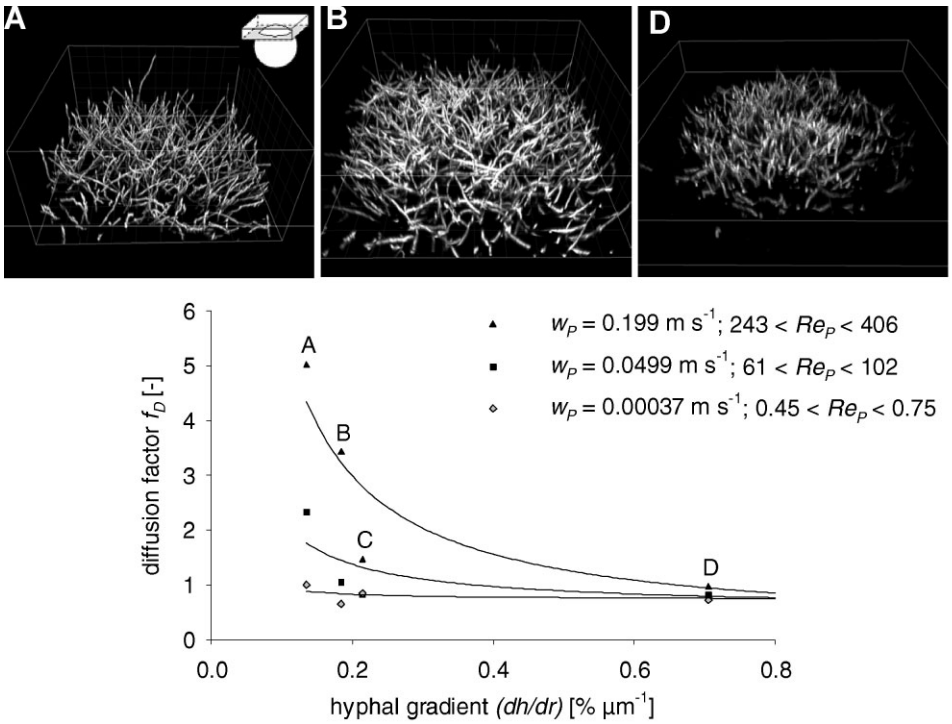

Figure 7. Three-dimensional reconstructions of CLSM-data (isosurface views) of the upper spherical cap of pellets A, B, and D and dependency of f_D (outer 200 µm pellet radius) on pellet morphology and fluid dynamics. Hyphae are stained with SYPRO Orange; edge length of boxes is 500 µm.

obtained by averaging CLSM-data of the pellet layer regarded (in this case, surface of the pellet to a depth of 200 µm) and given as 1 minus hyphal fraction in the range of 0–1. The other porosity ε_P was calculated based on pellet and hyphal density (Eq. 11) following the suggestion of Cui et al. (1998b) that again assumes a homogeneous biomass distribution in the pellet. As can be seen in Figure 8, despite the two different methods implemented, the porosities match very well. This can mainly be explained by the large volumetric fraction in the outer 200 µm radius with regard to the total pellet volume in these examples. Based on this fact, a porosity value close to the one of the whole pellet will be yielded. Additionally, it can be shown that the correlation between the diffusion factor and porosity is actually linear. However, the proportionality factor is 0.5 and thus does not equal 1, as would have been expected from Equation (10).

In Figure 9, the correlation of f_D with the hyphal gradient is shown. Here, a slight but significant decrease of the

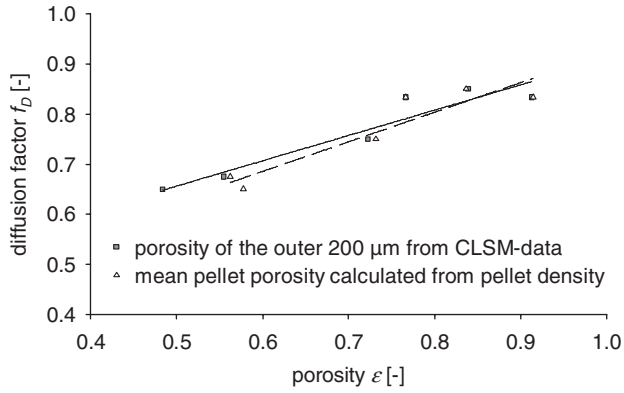

Figure 8. Correlation between ε and f_D for the outer 200 µm pellet radius. Measured at $1.5 < Re_P < 2.5$.

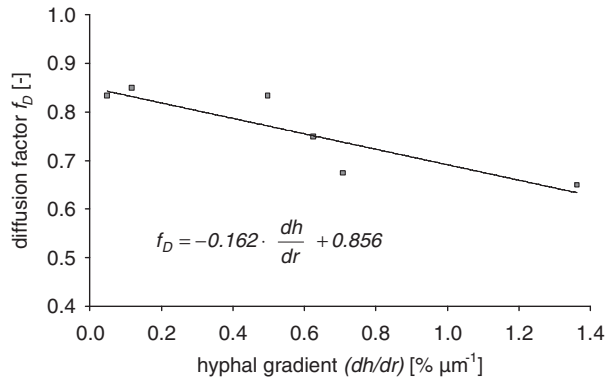

Figure 9. Correlation of (d*h*/d*r*) and f_D for the outer 200 µm pellet radius. Measured at $1.5 < Re_P < 2.5$.

diffusion factor with increasing sterical hindrance in the pellet periphery can be observed. From this correlation, f_D can be calculated as follows (Eq. 12)

$$f_D = \left(-0.162\left(\frac{dh}{dr}\right) + 0.856\right) \quad (12)$$

The results shown in Figure 9 correlate well with those of Cronenberg et al. (1994) for inactivated pellets of *P. chrysogenum*. As in this work, D_{eff} was determined numerically from the comparison of measured profiles and calculated response curves of a microelectrode positioned at a certain depth within a pellet. The main methodological deviation is the definition of the stimulus curve. In their work the concentration change of the mixed bulk phase is taken as the reference and therefore, external mass transfer resistances on the liquid side of the boundary "medium–pellet" (concentration boundary layer) are neglected. For small and dense pellets with largely homogeneous biomass distributions, a mean diffusion factor of 0.8 was found. The f_D of older pellets, which typically become less dense with time and exhibit layered morphology, was shown to be dependent on the position in the pellet. At the same time, the influence of advection on the internal mass transport increased. Overall, the diffusion factors obtained by Cronenberg et al. (1994) ranged between $0.6 < f_D < 5.45$, for a flow velocity at the pellets of $0.1\,m\,s^{-1}$. Considering this rather high velocity, their results can generally be confirmed by this investigation (see Fig. 7). Unfortunately, a quantitative correlation with pellet morphology is not provided in their article.

As the results of this work clearly demonstrate, the determination of diffusion factors in fungal pellets as an example of biological aggregates is still associated with several uncertainties. It was shown that the method chosen for determination significantly influences the results. It became particularly clear that the oxygen consumption of hyphae in viable pellets cannot be neglected. Diffusion factors measured in inactivated pellets through stimulus–response experiments are on average 30% higher than those determined in active pellets and those reported in literature. Nevertheless, these values are regarded as being fairly reliable since only transport processes, not conversion, are determined with this method. The results also confirm the theoretical assumption of a direct proportionality of the diffusion factor to pellet porosity. A linear correlation between diffusion factor f_D and hyphal gradient was found, with diffusion factors ranging between $0.65 < f_D < 0.85$. In the future, this correlation can be used to calculate oxygen mass fluxes for laminar flow conditions at the particle.

Investigations of the influence of hydrodynamic conditions on mass transport and turnover in fungal biopellets reveal that diffusion limitation in the pellet core occurs above a critical diameter of ~400 μm. However, diffusion limitation in the pellet periphery will only play a minor role for most hydrodynamic conditions in the range of practical relevance. For most cases it was shown that the external mass transfer resistance is negligible. Additionally, even at very low flow velocities advection contributed to mass transport in the regions supplied with oxygen. Therefore, diffusion factors well above one were determined which were shown to vary with the flow velocity. Of course, advective transport will most likely contribute to mass transport also in the cases where diffusion factors below one were found. The degree to which advection affects the mass transport certainly depends on pellet structure. Consequently, pure diffusive transport within the whole pellet is only to be expected in pellets having densely structured pellet peripheries when the flow conditions at the particle surface are laminar.

The mass transport mechanism at higher flow velocities, which tend to occur in submerged cultivations, is unknown. Therefore, investigations were made based on information from the microelectrode technique and CLSM to determine its effect on mass fluxes and, thus, the potential of hydrodynamics to increase turnover rates. Figure 10 shows an example of the spatially resolved profiles of both biomass and quasi-stationary oxygen concentrations in a pellet at two flow velocities. Biomass concentration was obtained by averaging the hyphal fraction within spherical shells of 10 μm thickness (radial coordinate) and multiplying it with a hyphal dry mass density of $220\,kg\,m^{-3}$. By the correlation of oxygen concentration with biomass concentration, denoted by the arrows in Figure 10, a local oxygen consumption rate $r_{O_2,n}$ $[kg\,m^{-3}\,s^{-1}]$ can be calculated for each spherical shell (Eq. 13). Here, simple Monod kinetics with oxygen as the sole limiting substrate was chosen. This is appropriate since the C-source and nutrients were supplied in excess in the experiments.

$$r_{O_2,n} = \frac{q_{O_2} c_{X,n} c_{O_2,n}}{c_{O_2,n} + K_{O_2}} \quad (13)$$

with K_{O_2} as the half saturation constant for oxygen (K_{O_2} = $0.1\,mg\,L^{-1}$ Kobayashi et al., 1973), $c_{X,n}$ and $c_{O_2,n}$ as the concentration of biomass and oxygen in a shell, respectively, and q_{O_2} as the biomass specific oxygen consumption

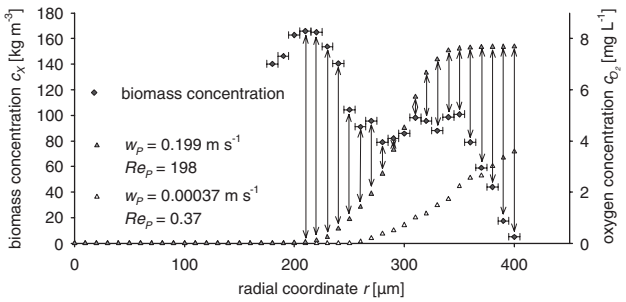

Figure 10. Biomass concentration profile (diamonds) and oxygen concentration profiles (triangles) determined at flow velocities at the pellet w_P of 0.00037 and $0.199\,m\,s^{-1}$, respectively. Arrows indicate combination of biomass and oxygen concentration (at $w_P = 0.199\,m\,s^{-1}$) in each spherical shell (see Eq.13).

rate [kg kg^{-1} s^{-1}]. q_{O_2} was determined to be $\sim$2.34 10^{-5} kg kg^{-1} s^{-1}, which is comparable to other values reported in literature [Hellendoorn et al., 1998; Rinas et al., 2005], and is assumed to be constant within the pellet periphery supplied with oxygen. This assumption will hold true for young to middle-aged pellets; however it could lead to overestimations of mass fluxes if an inactivation of hyphae occurs with increasing age. Thus, only those pellets were used for the calculations where this effect was not to be expected. Nevertheless, general differences in hyphal activity between pellets of different cultivations could not be considered. The sum of oxygen consumption within the spherical shells related to the pellet surface A_P then equals the mass flux into the pellet j_{rad}

$$j_{rad} = \sum_{1}^{n} \frac{r_{O_2,n} V_n}{A_P} \tag{14}$$

with V_n as the volume of the shell n.

In this way, j_{rad} can be determined without knowledge of the actual mass transport mechanism. Independent of how oxygen enters the pellet, from the measured oxygen profiles it can be determined how much oxygen is available for the hyphae at different depths within the pellet.

Figure 11 shows the mass fluxes j_{rad} dependent on pellet morphology for a flow velocity at the pellets of w_P = 0.199 m s^{-1} ($181 < Re_P < 485$). Additionally, mass fluxes j_l determined at laminar conditions at the particles ($Re_P < 1$), calculated according to Fick's first law (Eq. 4), are presented. Values of j_{rad} are up to three times higher than those of j_l, which can be ascribed to improved mass transfer as well as increased oxygen penetration depths due to advective transport. However, they seem to decrease drastically for pellets with loosely structured peripheries ($(dh/dr) < 0.75\%\ \mu m^{-1}$) which mechanistically, is difficult to explain. An important assumption on which the comparability of both slopes is based is an invariable pellet morphology. However, it was seen that pellets are compressed to a certain extent depending on their mechanical stability, as well as on the actual fluid dynamic stress. As mentioned before, especially in the case of fluffy pellets, hyphae which extend into the bulk phase are significantly bent by the fluid flow. As a result, the hyphae lie against the pellet surface and thereby increase the actual biomass density in the pellet periphery. The hyphal gradient, which is determined by CLSM analysis of suspended pellets in the absence of external forces, does not reflect this deformation. The quantified biomass distribution actually describes a morphology that in many cases might only occur at creeping flow conditions at the pellet. As a consequence, the penetration depth determined from the corresponding oxygen profile, which is needed for the calculation of the mass flux (Eq. 14) also does not factor in compression. If compression occurs, the amount of biomass being supplied with oxygen will be higher although penetration depths appear to remain fairly similar. It is consequently assumed that the actual mass fluxes, especially for pellets with low hyphal gradients, are underestimated. Since neither the extent to which compression occurs nor if compression can be completely neglected in very dense pellets is known, mass fluxes j_{rad} always represent conservative estimations.

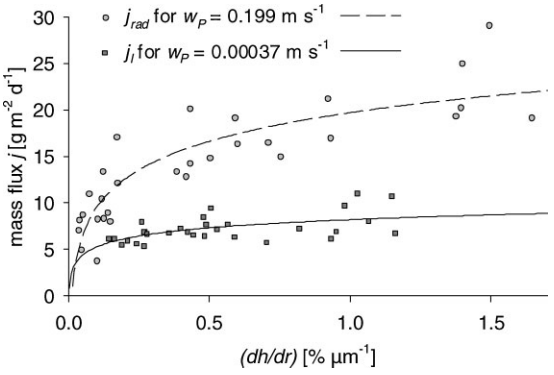

Figure 11. Mass fluxes j_{rad} (Eq.14) dependent on (dh/dr) for a flow velocity at the pellets of w_P = 0.199 m s^{-1} ($181 < Re_P < 485$) and in comparison to mass fluxes j_l (calculated according to Fick's first law (Eq.4)) for laminar flow conditions with a flow velocity at the pellets of w_P = 0.00037 m s^{-1} ($Re_P < 1$).

Concerning the influence of fluid dynamic conditions on mass fluxes, another conclusion can be drawn from Figure 11. Mass fluxes j_{rad} calculated at w_P = 0.199 m s^{-1} exhibit greater dependence on increasing hyphal gradients than those determined at w_P = 0.00037 m s^{-1}. This implies that turnover rates of pellets with denser peripheries can be significantly accelerated by increasing the flow velocity and thus, mass transfer. Although the penetration depth of oxygen in loosely structured pellets increases greatly with increasing relative velocity between the bulk phase and pellet, the additional amount of biomass supplied with oxygen can be significantly lower than in rather compact pellets. The radial coordinate also has an impact on this phenomenon. Since the penetration depth in fluffy pellets is high to begin with, it will be extended to regions in the pellet core that make up only a small fraction of the overall pellet volume. In denser pellets, the regions that will be additionally supplied with oxygen are smaller in terms of radial penetration but much closer to the pellet periphery and thus comprise not only a larger part of the pellet volume but also of its biomass. In summary, it can be stated that even without knowledge of mass transport mechanisms, mass fluxes in a pellet can still be estimated by combining radial oxygen and biomass concentration profiles.

Conclusion

Mass transport within fungal pellets is strongly dependent on pellet morphology as well as the actual fluid dynamic conditions at the pellet. The two methods introduced for determination of effective diffusivities of oxygen lead to very different results, which can be attributed to both, flow

velocities and influences of oxygen turnover. Measurements performed at defined fluid dynamic conditions in inactivated pellets proved to be most reliable. The experimental results obtained lead to the following conclusions:

- Diffusion as the sole transport mechanism within fungal biopellets can only be found at laminar flow conditions at the pellet and in very compact biopellet structures.
- Measurements in inactivated pellets reveal a negative correlation between the hyphal gradient—as a morphological parameter describing the pellet periphery—and the effective diffusion coefficient.
- Deformation of pellet structure has been underestimated in the past; it will clearly have a fundamental impact on penetration depths of substrates and, thus, the fraction of a pellet that is actually contributing to the pellet turnover.
- Coupling of microelectrode and CLSM techniques not only increases the understanding of transport processes, but also allows for the estimation of mass fluxes without knowledge of actual advective transport velocities.

Nomenclature

A_P	pellet surface area (m^2)
c_{O_2}	oxygen concentration ($kg\,m^{-3}$; $mg\,L^{-1}$)
c_X	biomass concentration ($kg\,m^{-3}$)
d	diameter (μm; m)
D_{eff}	effective diffusion coefficient ($m^2\,s^{-1}$)
D_{mol}	molecular diffusion coefficient ($m^2\,s^{-1}$)
(dc_{O_2}/dr)	spatial oxygen concentration gradient (radial) ($kg\,m^{-3}\,m^{-1}$)
$(dc_{O_2}/dr)_P$	spatial oxygen gradient at the pellet surface within the concentration boundary layer ($kg\,m^{-3}\,m^{-1}$)
$(dc_{O_2}/dr)_{max}$	maximum oxygen gradient within the pellet ($kg\,m^{-3}\,m^{-1}$)
(dc_{O_2}/dt)	temporal oxygen gradient ($kg\,m^{-3}\,s^{-1}$)
dh/dr	hyphal gradient in the pellet periphery ($\%\,\mu m^{-1}$)
f_D	diffusion factor
h	hyphal fraction (%)
j	mass flux ($g\,m^{-2}\,day^{-1}$; $kg\,m^{-2}\,s^{-1}$)
j_l	mass flux determined at laminar flow in the concentration boundary layer ($g\,m^{-2}\,day^{-1}$; $kg\,m^{-2}\,s^{-1}$)
j_{MK}	mass flux determined by microkinetics ($g\,m^{-2}\,day^{-1}$; $kg\,m^{-2}\,s^{-1}$)
j_{rad}	mass flux calculated by combination of oxygen and biomass concentration profiles ($g\,m^{-2}\,day^{-1}$; $kg\,m^{-2}\,s^{-1}$)
m_d	biomass dry weight (g; kg)
K_{O_2}	Monod constant for oxygen ($mg\,L^{-1}$)
q_{O_2}	biomass specific oxygen consumption rate ($kg\,kg^{-1}\,s^{-1}$)
r	radial coordinate (μm; m)
$r_{O_2,n}$	oxygen consumption rate per spherical shell n ($kg\,m^3\,s^{-1}$)
r_P	pellet radius (μm; m)
Re_{FC}	Reynolds number in the flow cell $Re_{FC} = w_a d_{FC}/\nu$
Re_P	Reynolds number at the particle, defined as $Re_p = w_p d_p/\nu$
t	time (s)
V_{MK}	liquid volume of microkinetics-cell
V_P	pellet volume (m^3)
w	flow velocity ($m\,s^{-1}$)
w_a	average flow velocity in a tube ($m\,s^{-1}$)
w_P	relative flow velocity at the particle/pellet ($m\,s^{-1}$)

Greek Symbols

ε	porosity
ε_P	pellet porosity
ν	kinematic viscosity ($m^2\,s^{-1}$)
ρ	pellet or aggregate density (dry biomass per wet pellet volume) ($kg\,m^{-3}$)
ρ_{BF}	biofilm density (dry weight) ($kg\,m^{-3}$)
ρ_H	hyphal density (dry weight) ($kg\,m^{-3}$)
ρ_P	pellet density (dry weight) ($kg\,m^{-3}$)

The authors gratefully acknowledge funding provided by the German Research Foundation through SFB 578 "Development of biotechnological processes by integrating genetic and engineering methods—From gene to product" at the Technische Universität Braunschweig.

References

Andrussow L. 1969. Diffusion. In: Borchers H, Hauser H, Hellwege KH, Schäfer K, Schmidt E, editors. Landolt-Börnstein. Zahlenwerte und Funktionen. Bd. II 5a. 6. Berlin: Springer-Verlag.

Bellgardt K-H. 1998. Process models for production of ß-lactam antibiotics. Adv Biochem Eng Biotechnol 60:153–194.

Bishop PL, Zhang TC, Fu Y-C. 1995. Effects of biofilm structure, microbial distributions and mass transport on biodegradation processes. Wat Sci Tech 31(1):143–152.

Cronenberg CCH, Ottengraf SPP, van den Heuvel JC, Pottel F, Sziele D, Schügerl K, Bellgardt KH. 1994. Influence of age and structure of *Penicillium chrysogenum* pellets on the internal concentration profiles. Bioproc Eng 10:209–216.

Cui YQ, van der Lans RGJM, Luyben KChAM. 1997. Effect of agitation intensities on fungal morphology of submerged fermentation. Biotechnol Bioeng 55(5):715–726.

Cui YQ, van der Lans RGJM, Luyben KChAM. 1998a. Effects of dissolved oxygen tension and mechanical forces on fungal morphology in submerged fermentation. Biotechnol Bioeng 57(4):409–419.

Cui YQ, Okkerse WJ, van der Lans RGJM, Luyben KChAM. 1998b. Modeling and measurements of fungal growth and morphology in submerged fermentations. Biotechnol Bioeng 60(2):216–229.

Elberling B, Damgaard LR. 2001. Microscale measurements of oxygen diffusion and consumption in subaqueous sulfide tailings. Geochim Cosmochim Acta 65(12):1897–1905.

El-Enshasy HA, Hellmuth K, Rinas U. 1999. Fungal morphology in submerged cultures and its relation to glucose oxidase excretion by recombinant *Aspergillus niger*. Appl Biochem Biotechnol 81(1):1–11.

Escamilla Silva EM, Gutierrez GF, Dendooven L, Jiménez IH, Ochoa-Tapia JA. 2001. A method to evaluate the isothermal effectiveness factor for dynamic oxygen into mycelial pellets in submerged cultures. Biotechnol Prog 17:95–103.

Fan L-S, Leyva-Ramos R, Wisecarver KD, Zehner BJ. 1990. Diffusion of phenol through a biofilm grown on activated carbon particles in a draft-tube three-phase fluidized-heat bioreactor. Biotechnol Bioeng 35:279–286.

Fu Y-C, Zhang TC, Bishop PL. 1994. Determination of effective oxygen diffusivity in biofilms grown in a completely mixed biodrum reactor. Wat Sci Tech 29(10–11):455–462.

Hamanaka T, Higashiyama K, Fujikawa S, Park EY. 2001. Mycelial pellet intrastructure and visualization of mycelia and intracellular lipid in a culture of *Mortierella alpina*. Appl Microbiol Biotechnol 56:233–238.

Hellendoorn L, Mulder H, van den Heuvel JC, Ottengraf SPP. 1998. Intrinsic kinetic parameters of the pellet forming fungus *Aspergillus awamori*. Biotechnol Bioeng 58(5):478–485.

Higashiyama K, Murakami K, Tsujimura H, Matsumoto N, Fujikawa S. 1999. Effects of dissolved oxygen on the morphology of an arachidonic acid production by *Mortierella alpina* 1S-4. Biotechnol Bioeng 63(4): 442–448.

Hille A. 2008. Stofftransport- und Stoffumsatzprozesse in filamentösen Pilzpellets. In Hempel, DC (editor): ibvt-Schriftenreihe, Band 32, FIT-Verlag Paderborn, at the same time dissertation, Technische Universität Carolo-Wilhelmina zu Braunschweig.

Hille A, Neu TR, Hempel DC, Horn H. 2005. Oxygen profiles and biomass distribution in biopellets of *Aspergillus niger*. Biotechnol Bioeng 92(5):614–623.

Horn H, Morgenroth E. 2006. Transport of oxygen, sodium chloride, and sodium nitrate in biofilms. Chem Eng Sci 61(5):1347–1356.

Huang MY, Bungay HR. 1973. Microprobe measurements of oxygen concentrations in mycelial pellets. Biotechnol Bioeng 24:1193–1197.

Kelly S, Grimm LH, Hengstler J, Schultheis E, Krull R, Hempel DC. 2004. Agitation effects on submerged growth and product formation of *Aspergillus niger*. Bioproc Biosys Eng 26(5):315–323.

King R. 1998. Mathematical modelling of the morphology of *Streptomyces* species. Adv Biochem Eng/Biotechnol 60:95–124.

Kobayashi T, van Denem G, Moo-Young M. 1973. Oxygen transfer into mycelial pellets. Biotechnol Bioeng 15:27–45.

Lejeune R, Baron GV. 1997. Simulation of growth of a filamentous fungus in 3 dimensions. Biotechnol Bioeng 53:139–150.

Lewis WK, Whitman WG. 1924. Principles of gas absorption. Ind Eng Chem 16:1215–1220.

Mattern IE, Noort JMv, Berg Pvd, Archer DB, Roberts IN, van den Hondel CAMJJ. 1992. Isolation and characterization of mutants of *Aspergillus niger* deficient in extracellular proteases. Mol Gen Genomics 234:332–336.

Miura Y, Miyamoto K, Kanamori T, Ohira N. 1975. Oxygen transfer within fungal pellets. J Chem Eng Jpn 8:300–304.

Reichert P. 1994. AQUASIM Computer Program for simulation and data analysis of aquatic systems. Schriftenreihe der EAWAG, Dübendorf, ISBN 3906484084.

Revsbech NP, Kjaer T, Damgaard LR, Lorenzen J, Larsen LH. 2000. Biosensors for analysis of water, sludge and sediments with emphasis on microscale biosensors. In: Buffle J, Horvai G, editors. In situ monitoring of aquatic systems. New York: John Wiley and Sons, Ltd. p 195–222.

Riley MR, Muzzio FJ, Buettner HM, Reyes SCA. 1995. Diffusion in heterogeneous media: Applications to immobilized cell systems. AIChE J 41:691–700.

Rinas U, El-Enshasy H, Emmler M, Hille A, Hempel DC, Horn H. 2005. Simulation of substrate conversion, product formation and mass transport in *Aspergillus niger* biopellets. Chem Eng Sci 60:2729–2739.

Sharon C, Nakazato M, Ogawa HI, Kato Y. 1999. Bioreactor operated production of lipase: Castor oil hydrolysis using partially purified lipase. Ind J Exp Biol 37:481–486.

Staudt C. 2005. Entwicklung der Struktur von Biofilmen. Dissertation, Technische Universität Carolo-Wilhelmina zu Braunschweig, FIT-Verlag, Band 22, ibvt-Schriftenreihe.

Wäsche S, Horn H, Hempel DC. 2002. Influence of growth conditions on biofilm development and mass transfer at the bulk/biofilm interface. Water Res 36(19):4775–4784.

Wittler R, Baumgärtl H, Schügerl K, Lübbers DW. 1984. Oxygen transfer in *Penicillium chrysogenum* pellets. 3rd Eur Congr Biotechnol: 513–520.

Wittler R, Baumgärtl H, Lübbers DW, Schügerl K. 1986. Investigations of oxygen transfer into *Penicillium chrysogenum* pellets by microprobe measurements. Biotechnol Bioeng 28:1024–1036.

Yano T, Kodama T, Yamada K. 1961. Fundamental studies on the aerobic fermentation Part 8: Oxygen transfer within a mold pellet. Agric Biol Chem 25(7):580–584.